Traffic-Aware Ecological Cruising Control for Connected Electric Vehicle

Bingbing Li, Weichao Zhuang, *Member*, *IEEE*, Hao Zhang, Hao Sun, Haoji Liu, Jianrun Zhang, Guodong Yin, *Senior Member*, *IEEE*, Boli Chen, *Member*, *IEEE*

***Abstract*—The advent of intelligent connected technology has greatly enriched the capabilities of vehicles in acquiring information. The integration of short-term information from limited sensing range and long-term information from cloud-based systems in vehicle motion planning and control has become a vital means to deeply explore the energy-saving potential of vehicles. In this study, a traffic-aware ecological cruising control (T-ECC) strategy based on a hierarchical framework for connected electric vehicles in stochastic traffic environments is proposed, leveraging the two distinct temporal-dimension information. In the upper layer that is dedicated for speed planning, a sustainable energy consumption strategy (SECS) is introduced for the first time. It finds the optimal economic speed by converting variations in kinetic energy into equivalent battery energy consumption based on long-term road information. In the lower layer, a synthetic rolling-horizon optimization control (SROC) is developed to handle real-time traffic stochasticity. This control approach jointly optimizes energy efficiency, battery life, driving safety, and comfort for vehicles under dynamically changing traffic conditions. Notably, a stochastic preceding vehicle model is presented to effectively capture the stochasticity in traffic during the driving process. Finally, the proposed T-ECC is validated through simulations in both virtual and real-world driving conditions. Results demonstrate that the proposed strategy significantly improves the energy efficiency of the vehicle.**

***Index Terms*—Eco-driving, Electric vehicles, Energy efficiency, Model predictive control, Intelligent connected technology.**

I. Introduction

Environmental pollution is a pressing global concern that poses significant challenges to sustainable development [1]. One of the most prominent pollutions is road traffic emissions, which contribute to air pollution and climate change [2]. The adverse effects of vehicle emissions on public health and the environment necessitate the exploration of effective strategies to mitigate the pollution [3]-[4]. In this context, eco-driving has emerged as a promising approach to improve energy efficiency, cut emissions as well as enhance traffic throughput [5]. It can be enabled by training drivers to operate vehicles in an energy-efficient way, i.e., avoiding unnecessary acceleration/deceleration, idling and stops in a signalized corridor, yet it may increase the operational burden on drivers and labor cost to society [6], [7]. As an alternative, designing a vehicle velocity control strategy (e.g., driver assistance systems) can also minimize vehicle energy consumption by optimizing the driving profile [8]-[14].

Up to now, numerous studies have been conducted to investigate and to evaluate various aspects of eco-driving strategies. Typically, the pulse and glide (PnG) strategy proposed by Li *et al.* [15] is recognized to have better energy efficiency performance than constant speed cruising on flat roads by the optimal control theory. Lin *et al.* [16] formulated an open-loop optimal control problem considering more realistic vehicle powertrain dynamics, an approximate solution was derived by employing two- or three-stage operation rules, resulting in improved fuel economy for the vehicle. Shan *et al.* [17] investigated the combined effect of bus stops and signalized intersections on the energy consumption of connected automated electric buses, and a comprehensive speed trajectory planning method balancing travel time and energy consumption was presented. Dong *et al.* [18] developed a predictive energy-aware driving strategy to minimize energy consumption for electric vehicles (EVs) crossing multiple signalized intersections. Compared to the constant speed (CS) strategy, the proposed method can reduce energy consumption by 19.98%. Yan *et al.* [19] designed an eco-coasting controller, which utilizes road information preview to calculate the optimal timing and duration for coasting maneuvers, and a tailored real-time mixed integer programming algorithm is proposed by the authors to achieve energy-efficient results that highly approximate the globally solutions from dynamic programming. Mousa *et al.* [20] first introduced a deep reinforcement learning strategy that mimics human learning behavior to avoid red light stops, achieving an average fuel saving of 13.02%. Unlike conventional eco-driving control methods that consider only longitudinal dynamics, Liu *et al.* [21] studied a lateral control strategy to improve vehicle economy during cornering scenarios. However, the studies mentioned above all assume that vehicles are operating under free-flowing traffic conditions.

In real-world traffic environment the dynamic nature of road

This work is supported by National Natural Science Foundation (NNSF) of China under Grants 52172383 and Postgraduate Research & Practice Innovation Program of Jiangsu Province under Grant KYCX22_0196. (*Corresponding author: Weichao Zhuang*)

B. Li, W. Zhuang, H. Liu, J. Zhang, G. Yin are with School of Mechanical Engineering, Southeast University, Nanjing, 211189, China. (e-mail: bingbli@seu.edu.cn, wezhuang@seu.edu.cn, hjl@seu.edu.cn, zhangjr@seu.edu.cn, ygd@seu.edu.cn.).

B. Chen, H. Sun are with the Department of Electronic and Electrical Engineering, University College London, WC1E 6BT London, U.K. (e-mail: boli.chen@ucl.ac.uk, h.sun.20@ucl.ac.uk.).

H. Zhang is with the State Key Laboratory of Automotive Safety and Energy, Tsinghua University, Beijing 100084, China. (e-mail: hao_thu@foxmail.com.).

conditions and traffic patterns significantly influences the energy economy of vehicles, thus, the availability of traffic information is essential to solving the problem of eco-driving. Of particular importance is the emergence of vehicle-to-vehicle (V2V) and vehicle-to-infrastructure (V2I) communication technologies, which enable vehicles to gather and exchange information [22], [23]. These advancements have opened new avenues for exploring and optimizing vehicle speed for improving energy efficiency. Zhu *et al.* [24] introduced an adaptive cruise control system based on back-stepping technology to achieve synergistic optimization of driving safety and vehicle economy in a networking environment. Bakibillah *et al.* [25] implemented a learning-based event-driven eco-driving system by using the automatic driving data of the vehicle to generate the optimal speed. Li *et al.* [26] presented a fuel consumption optimization algorithm with model predictive control (MPC) for intelligent networked vehicles in a car-following scenario. Ngo *et al.* [27] developed a real-time eco-driving strategy for EVs to generate a safe and economic speed profile while avoiding collisions and respecting speed limits. Although the aforementioned studies have achieved certain benefits, they mainly employ receding horizon optimization methods to improve energy efficiency by using short-term information only that tends to yield sub-optimal solutions. Furthermore, these optimization methods directly focus on minimizing fuel or energy consumption in a single layer of control, which poses significant challenges in terms of real-time computational efficiency, due to the continuous, non-quadratic, and highly nonlinear nature of the problem. To alleviate computational burden, some scholars have applied convex optimization techniques to energy consumption models. Jia *et al.* [28] and Lacombe *et al.* [29] transformed the problem from the time domain to the spatial domain, where the energy consumption model can be convexified. However, these approaches result in inadequate vehicle energy savings due to the mismatch in the energy consumption model. On the other hand, some scholars [30]-[32] have addressed the issue of computational efficiency by adopting an approach that involves tracking a constant maximum speed and adaptively adjusting the following distance to ensure safety. However, relying solely on a fixed target speed does not fully achieve the optimal economic driving, especially on roads with varying slopes. In addition, to the best of authors' knowledge, current eco-driving strategies mostly focus on deterministic and singular scenarios, which are either free-driving scenarios or car-following scenarios [33]-[35]. However, these approaches may be impractical for vehicles traveling long distances, as the preceding vehicle can appear at any location and time along the journey, and this necessitates an eco-driving strategy capable of accommodating the stochastic nature of traffic scenarios. Meanwhile, properly representing the stochastic characteristics of preceding vehicles is also crucial for achieving eco-driving in real-world scenarios.

Based on the state-of-the-art discussions, a layered control strategy, called traffic-aware ecological cruising control (T-ECC), is proposed to support energy-efficient vehicle driving for connected electric vehicle (CEV). The proposed method incorporates the global nature of long-term information and the dynamic nature of short-term information to achieve optimal performance in terms of energy efficiency, battery life, driving safety, and comfort for CEV. The performance of the proposed T-ECC is verified by a stochastic preceding vehicle model to evaluate the energy efficiency improvement compared to redesign CS strategies. In addition, a real-world experiment is conducted to validate the feasibility of T-ECC and the reliability of the simulation results. The contributions of this paper are threefold:

1) A full horizon energy-aware speed planning strategy, namely, sustainable energy consumption strategy (SECS), is developed in the eco-driving of CEV to find long-term speed plans by transforming vehicle kinetic energy into equivalent battery energy. The validated strategy, with the improvement in energy efficiency of real CEV, further opens new avenues of thought for eco-driving in EVs.
2) An optimal control strategy, synthetic rolling-horizon optimization control (SROC), is designed to conduct real-time velocity control subject to the speed plans determined in the upper layer in time-varying traffic conditions. Compared with the commonly used MPC-based method, the designed SROC enjoys both the merits of MPC and adaptive cruise control (ACC), striking the balance between computation efficiency and optimality.
3) A stochastic preceding vehicle model calibrated on real traffic data is designed to construct dynamic traffic scenarios for carrying out more realistic simulation trials.

The rest of this paper is organized as follows. Section II formulates the problem of ecological cruise control for EVs and establishes the system model. Section III describes the proposed T-ECC strategy. Stochastic simulations are conducted to evaluate the effectiveness of the proposed strategy in section IV. In section V, a real-world vehicle experiment is carried out to validate the T-ECC strategy. The paper is concluded in Section VI.

II. Problem Formulation

This section formulates the ecological cruise control problem of a CEV and introduces the modelling framework, including vehicle motion and powertrain models.

A. Problem Description

This paper investigates ecological cruise control on highways with diverse gradients in a stochastic driving environment, as illustrated in Fig. 1, where the state of the preceding vehicle is random, including the initial position, duration on the road and its velocity profile. Through the integration of V2I and V2V communication, a wealth of real-time traffic information can be efficiently obtained by CEV. This includes crucial data such as speed limits, road gradient, and the states of preceding vehicles, which are transmitted to the ego vehicle. The proposed strategy involves calculating the optimized speed to control the longitudinal motion of the ego vehicle. The primary objective of this strategy is to enhance energy efficiency of the ego vehicle, while extending the battery life and maintaining driving safety in the context of dynamic and random traffic

scenarios.

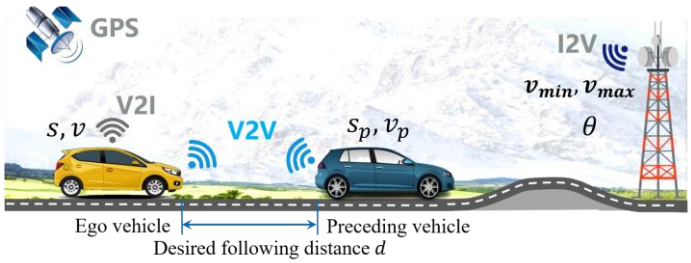

Fig. 1. Ecological cruising control on a highway with varying slopes.

B. Vehicle motion model

Considering that this paper focuses on the longitudinal performance of the vehicle, lateral movement is neglected. Thus, the longitudinal dynamics of a CEV traveling on a hilly road can be described by

$$\delta m a = F_t - F_r - F_g - F_i \tag{1}$$

with

$$F_r = mgf\cos(\theta) \tag{2a}$$

$$F_g = mg\sin(\theta) \tag{2b}$$

$$F_i = 0.5 C_d \rho A v^2 \tag{2c}$$

where δ is the vehicle rotational inertia coefficient, m is the vehicle mass, a is the vehicle acceleration. F_r, F_g and F_i are the rolling resistance, ramp resistance and air drag resistance, respectively. g is the gravity constant, f, θ, and C_d are the rolling resistance factor, gradient and aerodynamic drag factor, respectively. A is the frontal area, ρ is the air density. F_t is the traction force, originating from the power supplied by the motor and transferred to the vehicle wheels through its transmission system. The traction force can be described as

$$F_t = \frac{T i_g \eta_t}{r_w} \tag{3}$$

where T is the motor torque, i_g is the transmission ratio, η_t is the transmission efficiency of the powertrain, r_w is the tire rolling radius of the vehicle

C. Electric Motor Model

The subject vehicle is a commercial vehicle equipped with two PD18 in-wheel motors, and the efficiency data of the PD18 motors is provided by Protean Electric Inc. Based on the experimental data, a static lookup table is established to depict the driving and braking efficiency map of the motor, as depicted in Fig. 2. Hence, the power consumption of the entire propulsion system is characterized as follows [36]

$$P_e = 2P_m \eta_m^{-sgn(P_m)} = 2T\omega \eta_m^{-sgn(P_m)} \tag{4}$$

where P_e is the power consumption of propulsion system, P_m is the required motor power. When $P_m > 0$, it consumes energy as a motor to drive the vehicle, and when $P_m < 0$, it functions as a generator to recover electrical energy. $sgn(\cdot)$ is the sign function, and η_m, as depicted in Fig. 2, represents the motor working efficiency, which is related to the torque T and speed ω of the motor.

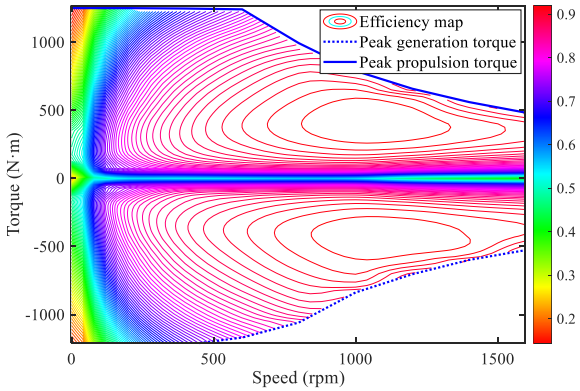

Fig. 2. Efficiency map and external characteristics of the electric motor.

D. Battery model

The power source of the ego vehicle comes from a battery composed of a batch of LiFePO4 cells. The battery not only provides the drive energy consumption for the powertrain, but also supplies energy for the vehicle accessory, such as air conditioning, lighting, etc. Therefore, the terminal battery power P_b can be defined as

$$P_b = P_e + P_{aux} \tag{5}$$

where P_{aux} is the auxiliary power.

To characterize the battery dynamics of ego vehicle, an equivalent electrical circuit is used to model the lithium-ion phosphate battery system [37], where the complex electrochemical reaction inside the battery is ignored, and only the charge and discharge characteristics of the battery are considered. The battery model is hence given by

$$P_b = U_{oc} I_b - I_b^2 R_b \tag{6}$$

where I_b is the battery current. U_{oc} and R_b are the open-circuit voltage and internal resistance of the battery, respectively. For each LiFePO4 cell, its open circuit voltage and internal resistance are defined as functions of battery state of charge (SOC) shown in Fig. 3.

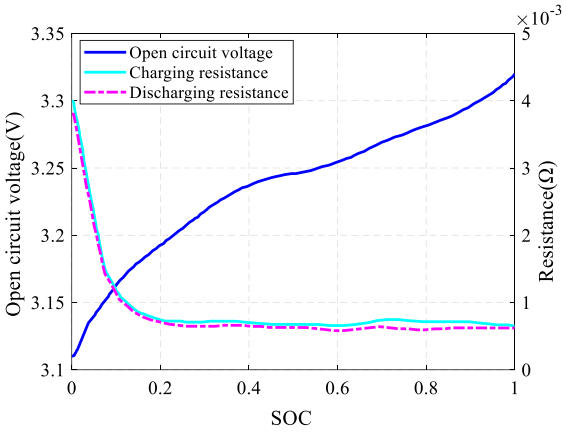

Fig. 3. SOC-dependent battery resistance and open circuit voltage.

The dynamics of SOC is described as

$$\dot{SOC} = -\frac{I_b}{Q_b} = -\frac{U_{oc} - \sqrt{U_{oc}^2 - 4R_b P_b}}{2Q_b R_b} \tag{7}$$

where Q_b is the nominal capacity of the battery.

Battery aging is an important performance metric that influces the capacity. In this study, a semi-empirical model

based on experimental data is employed to describe the battery degradation [38]. This model delineates that the predominant factors influencing battery aging are the discharge/charge rates and the depth of discharge. It is characterized by an equation representing battery capacity loss, which can be expressed as

$$Q_{loss} = B \cdot \exp\left(\frac{-E_a(I_c)}{R_a T_b}\right) \cdot \left(\frac{\int |I_b| dt}{3600}\right)^z \quad (8)$$

where Q_{loss} is the battery capacity loss, B is the pre-exponential factor, E_a is the activation energy related to the instantaneous battery discharge/charge rate I_c, where $E_a = 31700 - 370.3I_c$ and $I_c = I_b/C_b$, C_b is the cell capacity. R_a is the gas constant, T_b is the ambient temperature, z is the power law factor.

III. Traffic-Aware Ecological Cruising Control Strategy Design

To balance the proportions of optimality and computational efficiency, a hierarchical T-ECC strategy is presented, as depicted in Fig. 4. In addition, the construction of stochastic traffic scenarios is also shown in this section.

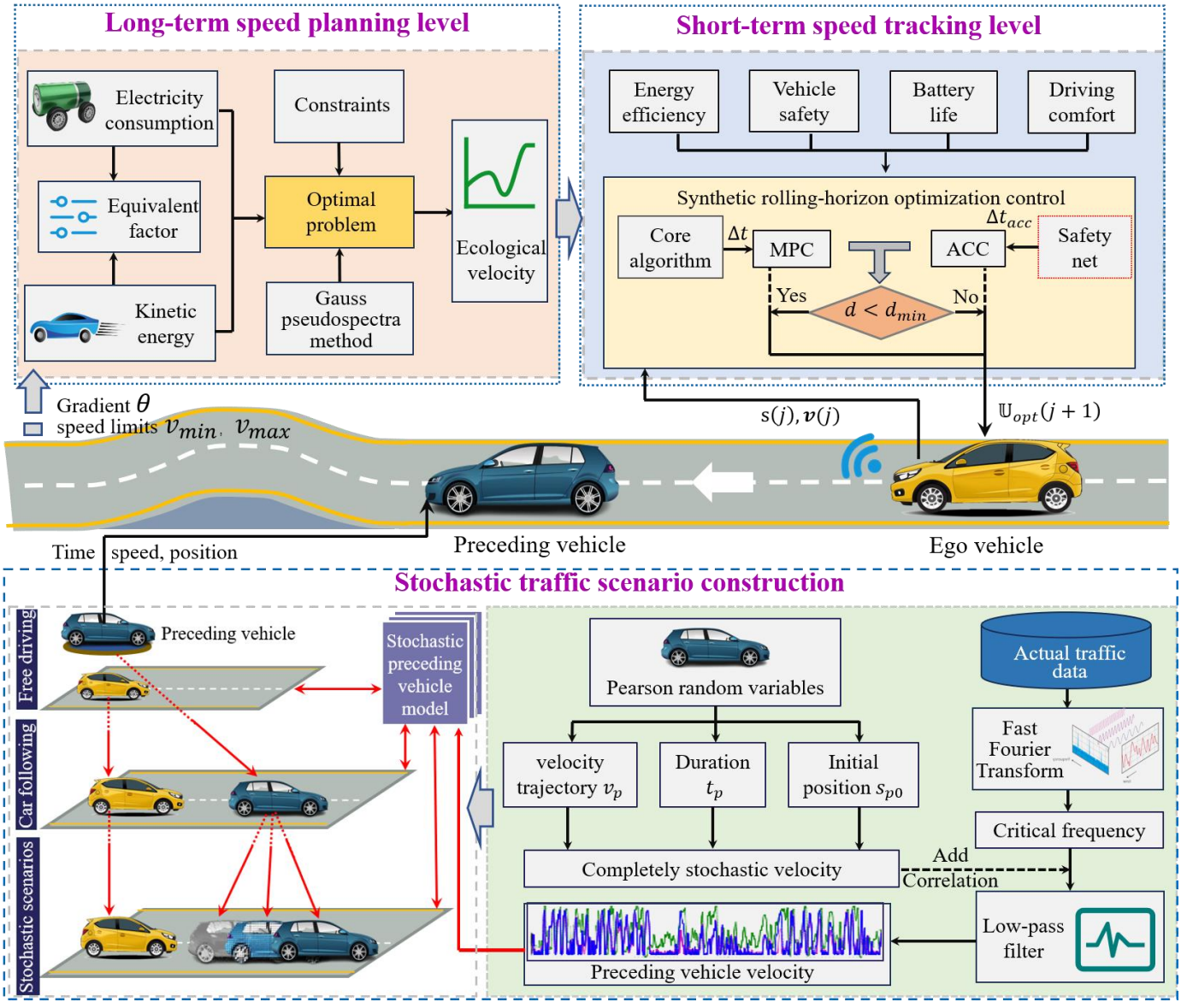

Fig. 4. Schematic framework of the proposed T-ECC.

A. Sustainable Energy Consumption Strategy

For the upper-level speed planning, a SECS based on deterministic long-term information, such as destination location and road gradient information, is developed in T-ECC. The proposed SECS is a full horizon planning strategy, inspired by Li's PnG strategy, which states that the vehicle body functions as an energy store to facilitate the efficiency of the internal combustion engine. Based on this finding, we regard the kinetic energy of the vehicle body as energy reserve in the same way as battery energy with effective power splitting rules to minimize the equivalent energy consumption of the system. Further, to realize the energy distribution of kinetic energy and battery power in EVs, the equivalent consumption minimization strategy (ECMS) [39] idea for hybrid vehicles is introduced into the speed planning of EVs. In ECMS, the power distribution strategy between the internal combustion engine

and the electric motor is optimized by minimizing the equivalent consumption, which is composed of transient fuel consumption and electricity. In addition, converting the longitudinal model from the temporal domain to the spatial domain will enable effective energy optimization, because most of the environmental characteristics associated with traffic conditions can fluctuate spatially [28]. For instance, the velocity v and the road gradient θ are stated as $v(s)$ and $\theta(s)$, respectively. Further, denoting the traveled distance by s and the trip time by t, a function dv/ds can be defined as follows

$$\frac{dv}{ds} = \frac{dv}{dt} \cdot \frac{dt}{ds} = \frac{1}{v} \cdot \frac{dv}{dt} \tag{9}$$

Therefore, the equivalent energy consumption rate of SECS is formulated as

$$E_{secs} = \frac{E_e - \lambda E_k}{\Delta s} = \frac{2P_e}{v} - \lambda ma \tag{10}$$

with

$$E_e = \int_{s_0}^{s} \frac{P_b(s)}{v(s)} ds \tag{11a}$$

$$E_k = \int_{s_0}^{s} \frac{m\left(v^2(s) - v_0^2(s)\right)}{2} ds \tag{11b}$$

where E_{secs} is the equivalent energy consumption rate, E_e is the electricity consumption, E_k is the kinetic energy variation of the vehicle, s_0 is the initial position of a journey, v_0 is the initial speed, λ is the equivalent factor (EF) defined by (12) and (13), which is derived from numerical tests.

$$\lambda = 1 - \xi \cdot (\sigma - 0.5\Theta_v) \cdot \Theta_v^3 \tag{12}$$

$$\Theta_v = \frac{v - 0.5(v_{max} + v_{min})}{v_{max} - v_{min}} \tag{13}$$

where v_{max} and v_{min} are the maximum and minimum vehicle speed, respectively. Θ_v is the intermediate variable, σ and ξ are the manipulated parameters with the following constraints

$$0.5 < \sigma < 1 \tag{14a}$$

$$1 \leq \xi \tag{14b}$$

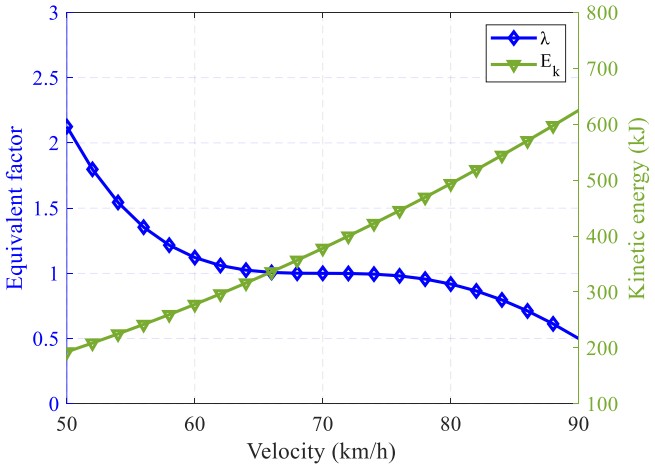

Fig. 5. Profiles of EF and vehicle kinetic energy against vehicle speed.

It can be seen from the above equation that the EF is a function of the vehicle speed v, influenced by the parameters ξ and σ. For an insight into the implications of SECS, we assume $\xi = 10$, $\sigma = 0.65$, and obtain the profile of the EF and kinetic energy against vehicle speed, as shown in Fig. 5. The profiles indicate that increasing speed leads to an increase in the kinetic energy of the vehicle, at which stage the EF decreases, which encourages reducing the kinetic energy of the vehicle body to offset the battery consumption, and vice versa. As such, the conceptual diagram of SECS is illustrated in Fig.6. The vehicle accelerates before going uphill in order to utilize its kinetic energy to overcome gravitational potential energy and avoid losing speed. Additionally, the vehicle releases kinetic energy when driving downhill, preventing unnecessary acceleration to reduce battery energy wastage.

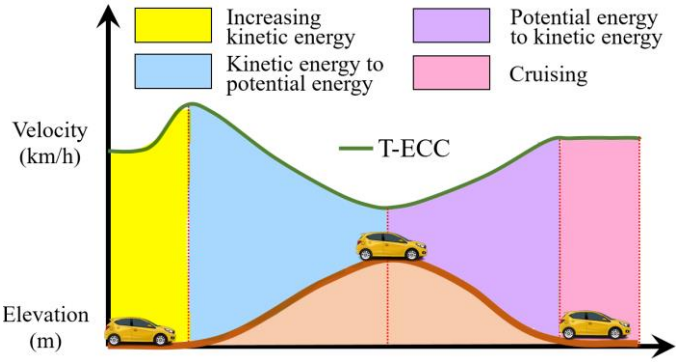

Fig. 6. Conceptual diagram of SECS.

Finally, the upper-level velocity planning is defined as an optimal control problem in the spatial domain as follows

$$\min_{T \in u} J = \int_{s_0}^{s_f} \underbrace{\left(\frac{P_b(T,v)}{v} - \lambda ma\right)}_{L(x,u,s)} ds \tag{15}$$

s.t.

$$\dot{x} = f(x,u) = \begin{bmatrix} \dot{v}(s) \\ \dot{t}(s) \end{bmatrix} = \begin{bmatrix} \frac{1}{\delta m v}\left(F_t - F_r - F_g - F_i\right) \\ 1/v \end{bmatrix} \tag{16a}$$

$$h(x,u,s) = \begin{bmatrix} v_{min} - v \\ v - v_{max} \\ T_{min} - T \\ T - T_{max} \\ a_{min} - a \\ a - a_{max} \end{bmatrix} \leq 0 \tag{16b}$$

where $L(x,u,s)$ is the cost function, $x = [v,t]^{\mathrm{T}}$ is the state variable, $u = T$ is control variable, s_0 and s_f are the start and end points respectively. Equation (16a) are the system dynamics in spatial domain. Equation (16b) collects the input and state constraints of the system. T_{min} and T_{max} are the minimum and maximum motor torque, respectively. a_{min} and a_{max} denote the minimum and maximum vehicle accelerations, respectively.

To alleviate the computational burden of (15), the Gauss pseudospectral method (GPM) is used to address the above problem, which transforms the continuous optimal control problem into a discrete nonlinear programming problem (NLP), which can be solved by a well-developed algorithm [40]. In GPM, (15) is rewritten as

$$J = \frac{s_f - s_0}{2} \int_{-1}^{1} \mathcal{L}(x(\tau), u(\tau), \tau) d\tau \tag{17}$$

with

$$s = \frac{s_f - s_0}{2}\tau + \frac{s_f + s_0}{2}, \tau \in [-1,1] \tag{18}$$

Next, the discrete and approximate state and input variables are performed. Define Legendre-Gauss points τ_i, where $i = 1, 2, \cdots, N$. Thus, the states variables X and control variables U are discretized as

$$\begin{cases} X = [x(\tau_0), x(\tau_1), x(\tau_2), \cdots, x(\tau_N)] \\ U = [u(\tau_0), u(\tau_1), u(\tau_2), \cdots, u(\tau_N)] \end{cases} \tag{19}$$

The Lagrange interpolation are used to approximate the state variables and control inputs at collocations points, i.e.,

$$\begin{cases} x(\tau) \approx \sum_{i=0}^{N} L_i(\tau)\, X_i \\ u(\tau) \approx \sum_{i=0}^{N} L_i(\tau)\, U_i \end{cases} \tag{20}$$

where $L_i(\tau)$ are the Lagrange basis polynomials, that is,

$$L_i(\tau) = \prod_{j=0, j\neq i}^{N} \frac{\tau - \tau_i}{\tau_i - \tau_j} \tag{21}$$

Then, the state variable differentiation can be derived from

$$\dot{x}(\tau) \approx \sum_{i=0}^{N} \dot{L}_i(\tau)\, X_i = \sum_{i=0}^{N} D_{ki}\, X_i, k = 1, 2, \cdots, N \tag{22}$$

where D_{ki} is the differential approximation matrix. Further, the state transfer equation of the system can be rewritten in algebraic constraints form as follows

$$\begin{cases} XD_k = \frac{s_f - s_0}{2} f(X_k, U_k) \\ X_k \equiv x(\tau_k), U_k \equiv u(\tau_k) \end{cases} \tag{23}$$

In addition, based on the Gaussian-Lobatto quadrature, the cost function is converted into

$$J = \frac{s_f - s_0}{2} \sum_{k=0}^{N} \omega_k \mathcal{L}\big(x(\tau_k), u(\tau_k)\big) \tag{24}$$

After the aforementioned steps, the whole optimal control problem based on the GPM is transformed into

$$J = \frac{s_f - s_0}{2} \sum_{k=0}^{N} \omega_k \mathcal{L}\big(x(\tau_k), u(\tau_k)\big) \tag{25}$$

s.t.

$$XD_k = \frac{s_f - s_0}{2} f(X_k, U_k) \tag{26a}$$

$$h(X_k, U_k) \leq 0, k = 1, 2, \cdots, N \tag{26b}$$

The resulting NLP can be addressed using the sequential quadratic programming approach because it is effectively a high-dimensional sparse optimization issue [41]. After above process, the free-flow velocity-optimal trajectory is obtained v_{eco}.

B. Synthetic Rolling-horizon Optimization Control

In the lower layer, to cope with the disturbances from preceding vehicles in stochastic road conditions, a SROC approach combined ACC and MPC is applied to track ecological vehicle speeds planned by the SECS, while ensuring vehicle safety, driving comfort, traffic efficiency and battery life.

In SROC, when the preceding vehicle emerges from a certain range in front of the ego vehicle, a minimum following distance is defined by the intelligent driver model (IDM) for vehicle safety [42]-[44], i.e.,

$$d_{min} = d_0 + vh_m + \frac{v(v - v_p)}{2\sqrt{a_{max} b}} \tag{27}$$

where d_0 is the static spacing between vehicles, h_m is the safe time headway, v_p is the speed of preceding vehicle, a_{max} and b are the maximum acceleration and the comfortable deceleration, respectively. Restricting only the minimum following distance for ego vehicle may lead to excessive following gaps, which are detrimental to traffic efficiency. Therefore, we have also set a maximum following distance [26]

$$d_{max} = 10 + v + 0.0825v^2 \tag{28}$$

As for a car-following process, the generally desirable following distance [45] can be given by

$$d_{des} = d_0 + vh_d \tag{29}$$

where h_d is the desired time headway. Hence, the cost function associated with safety and traffic throughput is defined as follows

$$J_d = \begin{cases} +\infty & d < d_{min} \\ f_1(d_{des} - d)^2 & d_{min} \leq d < d_{des} \\ f_2(d - d_{des})^2 & d_{des} \leq d < d_{max} \\ f_3(d - d_{max})^2 + f_2(d_{max} - d_{des})^2 & d_{max} \leq d \end{cases} \tag{30}$$

where d is the actual following distance, f_i ($i = 1, 2, 3$; $f_3 \gg f_2$) is the cost coefficients, which are set to 2, 1, and 50, respectively.

From the above, by combining energy efficiency, battery life, vehicle safety, driving comfort and traffic efficiency, the cost function over each moving horizon of MPC is formulated as

$$\min_u J(k) = \sum_{i=k}^{K+N_p-1} w_1 \big(v(k) - v_{eco}(k)\big)^2 + w_2 |\dot{a}(k)|^2 + w_3 J_d(k) + w_4 Q_{loss}(k)\Delta t \tag{31}$$

s.t.

$$s(k+1) = s(k) + \frac{v(k+1) + v(k)}{2}\Delta t \tag{32a}$$

$$v(k+1) = v(k) + a(k)\Delta t \tag{32b}$$

$$a(k) = \frac{1}{\delta m} \cdot \big(F_t(k) - F_r(k) - F_g(k) - F_i(k)\big) \tag{32c}$$

$$v_{min} \leq v(k) \leq v_{max} \tag{32d}$$

$$T_{min} \leq T(k) \leq T_{max} \tag{32e}$$

$$a_{min} \leq a(k) \leq a_{max} \tag{32f}$$

where the state variable is $x = [s, v]^T$, the control input is T. w_i ($i = 1, 2, 3, 4$) is weight factors. k is the current time step, N_p is the preview horizon length, Δt is the time step length.

It should be noted that in the discrete-time MPC, in general Δt is not setup in a small scale on account of the computational burden. However, during the car-following process, an emergency brake could happen in two consecutive time steps, leading to a serious safety accident. Therefore, in SROC, the continuous ACC [46] is provided as an additional safety assistance, which is operated in parallel with the MPC. For the

ACC, to ensure absolute safety, the following distance is formulated as

$$d_{acc} = d_0 + v(k)h_a \tag{33a}$$

$$d_{min} < d_{acc} < d_{des} \tag{33b}$$

where h_a is the time headway. In particular, smaller time steps for the ACC, i.e., $N_a \cdot \Delta t_{acc} = \Delta t$. The ACC here is based on the design of a PD controller. Finally, the whole SROC strategy schematic is presented, as shown in Fig. 7, where ACC is activated to act as a safety net for guaranteeing safe following distance only when $d < d_{min}$, i.e., by the control input of the ACC to prevent the possibility of a collision caused by unexpected braking of the preceding vehicle in-between time steps of the MPC. The pseudo-code for the SROC strategy is illustrated as Algorithm 1.

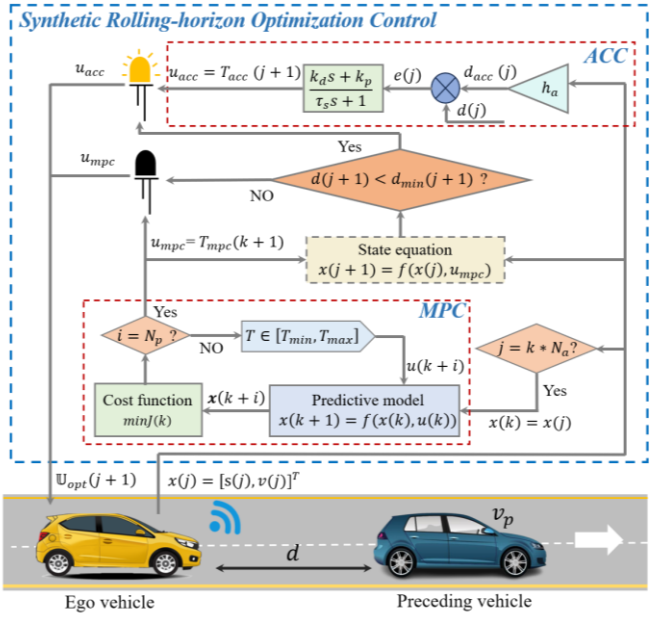

Fig. 7. The schematic of the SROC strategy.

Alogrithm 1 Implementation algorithm for SROC

Input: s_p, v_p, θ, v_{eco}

Output: $\mathbb{U}_{opt}$

1: Initialization by setting $x(j) = [s(j), v(j)]^T$, $T_{acc}(j)$, $T_{mpc}(j)$, v_{min}, v_{max}, T_{min}, T_{max}, a_{min}, a_{max}, d_0, d_0, h_m, h_a, h_d, Δt, Δt_{acc}, N_a, N_p
2: $j = j + 1$
3: **If** $j\%N_a == 0$ or $j == 0$
4: $x(k) = [s(j), v(j)]^T$
5: **For** $i = 0{:}1{:}N_p - 1$
6: Update $t \leftarrow t + \Delta t$
7: Update ego-vehicle's status by Eq(32a), (32b) and (32c) $x(k+i) \leftarrow f(x(k), u(k))$
8: Compute optimal control inputs $T_{mpc}(k+i)$
9: Go back to step 5
10: **End For**
11: $u_{mpc} = T_{mpc}(k+1)$
12: **End IF**
13: **Else**
14: Update $t \leftarrow t + \Delta t_{acc}$
15: Compute optimal control $u_{acc} = T_{acc}(j+1)$ by ACC
16: **End Else**
17: $x(j+1) \leftarrow f(x(j), u_{mpc})$
18: **If** $d(j+1) < d_{min}(j+1)$
19: $u(j) = u_{mpc}$
20: **Else**
21: Go back to step 2
22: Return $\mathbb{U}_{opt} = u(j)$

C. Stochastic Preceding Vehicle Model

To characterize a real long-distance driving scenario where the preceding vehicle may appear anytime and anywhere, a stochastic preceding vehicle model is developed in this paper. In this model, a random number generator first generates an arbitrary motion state of the preceding vehicle, then the critical frequency of the velocity signal in the real environment is determined based on the collected traffic data, eventually, the temporal correlation of the velocity is introduced by designing a Butterworth low-pass filter.

The initial position of the preceding vehicle s_{p0}, the duration on the road t_p and the preceding vehicle's velocity trajectory v_p are generated as Pearson random variables by means of a random number generator, and the random properties of these variables are calibrated using actual driving data. Notice that the simulated velocity trajectory of the preceding vehicle is discrete and random instead of being significantly correlated in the adjacent temporal domain for real driving conditions. Therefore, it is necessary to enhance the temporal correlation of v_p. We transform the random velocity from the time domain to the frequency domain, and for a time-discrete sequence of velocities $v_p[n]_{0 \le n \le N}$, its discrete Fourier transform is given by

$$V[k] = \sum_{n=0}^{N-1} e^{-j\frac{2\pi}{N}nk} v_p[n] \tag{34}$$

where $0 \le k \le N-1$, equation (34) is expanded as

$$V[k] = \sum_{n=0}^{N-1} v_p[n] \cdot \left[\cos\left(\frac{2\pi}{N}kn\right) - jsin\left(\frac{2\pi}{N}kn\right)\right] \tag{35}$$

It can be seen that the time complexity of Eq. (33) is $O(N^2)$. To improve computational efficiency, the Fast Fourier Transform (FFT) is employed, which reduces the time complexity to $O(NlgN)$ [47]. In FFT, we assume that $n = 2^m$. Equation (35) can be reformulated as

$$\begin{aligned} V[k] &= \sum_{r=0}^{\frac{N}{2}-1} e^{\frac{-2j\pi(2r)k}{N}} v_p[2r] + \sum_{r=0}^{\frac{N}{2}-1} e^{\frac{-2j\pi(2r+1)k}{N}} v_p[2r+1] \\ &= \underbrace{\sum_{r=0}^{\frac{N}{2}-1} e^{\frac{-2j\pi rk}{N/2}} v_p[2r]}_{A[k]} + e^{\frac{-2j\pi k}{N}} \underbrace{\sum_{r=0}^{\frac{N}{2}-1} e^{\frac{-2j\pi rk}{N/2}} v_p[2r+1]}_{B[k]} \end{aligned} \tag{36}$$

where $A[k]$ and $B[k]$ are even-numbered and odd-numbered data points, respectively. From this, we can obtain

$$V[k] = A[k] + e^{\frac{-2j\pi k}{N}} B[k] \tag{37}$$

The critical frequency of the real traffic data can be obtained by the FFT, which helps us to determine the retained frequency components of the velocities generated by the random number generator. Further, a Butterworth low-pass filter is designed to

introduce time dependence by selecting the cut-off frequency (i.e., filter time constant).

Alogrithm 2 The FFT algorithm

Input: velocity signal v_p, sampling rate Δt_{FFT}
Output: critical frequency F_c
1: Compute the signal length n_v
2: Perform fast fourier transform $V[k] \leftarrow v_p[n]$
3: Compute the frequency axis $F[n] \leftarrow (n, \Delta T)$
4: Find the index of the maximum magnitude $n_p \leftarrow (F[n], V[k])$
5: Get the corresponding critical frequency F_c
6: **End**

IV. Simulation and Discussion

In this section, the effectiveness of the proposed T-ECC is verified by several simulations. Note that all simulations are carried out on a workstation with Intel® Core™ i7-10875H CPU and 16 GB RAM.

A. Simulation Setup

To validate the devised strategy, it is imperative to establish a simulation environment that incorporates real world road data. Our selection for this purpose is an urban expressway situated in the northern region of Nanjing, China, as depicted in Fig. 8. Spanning a length of 30 km, this expressway serves as an ideal candidate. To capture the elevation information of this specific road segment, the Google elevation API is leveraged [48], which provides accurate and reliable data. In the simulation, relevant data for the subject vehicle, including the vehicle body, motor, and battery, are summarized in Table I. In addition, other parameters related to the proposed strategy and the simulation are provided in Table II.

In the simulation, to better represent the stochasticity of the forward traffic environment in ego vehicle driving, we simulate 1000 stochastic driving conditions by the developed stochastic preceding vehicle model and verify the performance of T-ECC under free-driving, car-following, and stochastic scenarios (i.e., the preceding vehicle may appear at any position of the journey). In contrast, a common CS strategy [49] is recognized as a benchmark, notably, the IDM is applied in CS to maintain safe following distance in response to time-varying traffic. For the sake of fairness, different comparison groups are set up for CS, i.e., speeds of 50 km/h, 60 km/h, 70 km/h, 80 km/h, and 90 km/h, named CS-1, CS-2, CS-3, CS-4, and CS-5, respectively.

Fig. 8. The experimental route in Nanjing City, China.

TABLE I
EGO VEHICLE PARAMETERS

Component	Parameter	Symbol	Value
Vehicle	Mass	m	2000 kg
	Accessory power	P_{aux}	400 W
	Rotational inertia coefficient	δ	1.022
	Tire radius	r_w	0.36 m
	Transmission efficiency the powertrain	η_t	0.95
	Frontal area	A	2.45 m^2
	Air-dragging resistance coefficient	C_d	0.28
	Transmission ratio	i_g	1
	Rolling resistance coefficient	f	0.015
	Air density	ρ	1.202 kg/m^3
	Gravity factor	g	9.81 m/s^2
Motor	Maximum Torque	T_{max}	1225 Nm
	Maximum Speed	ω_{max}	1600 rpm
Battery	Pre-exponential factor	B	-1516
	Gas constant	R_a	8.314
	Ambient temperature	T_b	298 K
	Power law factor	z	0.824
	Cell capacity	C_b	25 Ah

TABLE II
ALGORITHM PARAMETERS

Parameter	Symbol	Value
Sampling distance	Δs	2 m
Minimum speed	v_{min}	50 km/h
Maximum speed	v_{max}	90 km/h
Maximum acceleration	a_{max}	2 m/s^2
Maximum deceleration	a_{min}	-4 m/s^2
Static spacing	d_0	4.5 m
Safe time headway	h_m	1.5 s
Comfortable deceleration	b	-2.5 m/s^2
Desired time headway	h_d	2.5 s
Sampling time interval	Δt	1 s
Prediction horizon of MPC	N_p	10
Time headway of ACC	h_a	1 s
Sampling horizon of ACC	N_a	10
Sampling interval of ACC	Δt_{acc}	0.1 s

B. Simulation Results

1) Free-driving scenario

The vehicle speed profile for the T-ECC is depicted in Fig. 9. It can be easily observed that the speed of the T-ECC varies with road slope. Before climbing uphill, the vehicle accelerates in advance to store kinetic energy. This kinetic energy is then released while going uphill to offset the increase in gravitational potential energy. At the highest point of the road slope, the vehicle has the lowest speed. Then, the gravitational potential energy is converted into kinetic energy to reduce battery energy consumption. This is consistent with our proposed SECS superiority. It is this variation in speed that achieves energy savings and extended battery life for the vehicle, as confirmed in Table III. Table III demonstrates the average speed of the T-ECC is 69.2 km/h, improving energy efficiency by 8.56% and battery life by 17.6% compared to the similarly fast CS-3. Compared to other CS strategies, the improvement in vehicle energy efficiency is significant as the speed of the CS increases, together with a significant reduction in battery capacity loss and extended battery life. Despite CS-1 consumes less energy by driving at a much lower average speed, the T-ECC can save 28.3% travel time and 8.7% battery life.

To illustrate the energy saving mechanism of T-ECC, the motor torques of CS-1, CS-3, CS-5 and T-ECC are compared in Fig. 10. It is observed that the torque fluctuation of T-ECC is smoother and the braking frequency of the motor is significantly reduced, resulting from the SECS strategy in T-ECC, which increases the speed of the vehicle by converting kinetic energy, effectively avoiding the energy wastage caused by braking. Meanwhile, T-ECC exhibits a jump from low torque to high torque during vehicle drive. Further, we compare the motor output power distribution of the T-ECC and CS-3. Fig. 11 reveals that the output power of the CS-3 follows a normal distribution, while the distribution of the T-ECC is loosely distributed. In addition, the maximum and median values of motor output power for the T-ECC are smaller than the CS-3.

Finally, Fig. 12 indicates the distribution of motor operating states for CS-3 and T-ECC, which we classify the motor operating states as driving, coasting and braking. It is observed that CS-3 has a higher proportion of driving and braking, reaching 55.7% and 35.1% respectively, yet the proportion of coasting is only 9.2%. In contrast, the T-ECC is in the coasting zone for 36.7% of the journey when the vehicle is driven with sufficient energy consumption, suggesting that energy efficiency of the vehicle is more favorable in coasting conditions, which has been verified in the literature [50].

2) *Car-following scenario*

In 1000 sets of simulations, one simulation is randomly selected to verify effectiveness in a car-following scenario, where the vehicle enters a car-following area at 10 km to follow the preceding vehicle trajectory generated by the stochastic preceding vehicle model. Fig. 13 presents the longitudinal velocity profiles of the ego vehicle and the preceding vehicle in the car-following zone between 10 and 15 km of the road. It is noticeable that the ego vehicle tracks the speed trajectory of preceding vehicles well, and also that it decelerates more by coasting to avoid excessive braking, which facilitates driving comfort and economy of the ego vehicle. At 14 km of the journey, causing ego vehicle to perform a significant emergency braking maneuver for safety. However, shortly thereafter, ego vehicle gradually resumes following the preceding vehicle in a steady manner.

The following distance between the preceding vehicle and ego vehicle is displayed in Fig. 14. In Fig. 14, the actual following distances fluctuate between the maximum and minimum inter-vehicle distance, which demonstrates that the proposed following strategy of T-ECC is consistent with expectations. As shown in Table IV, the T-ECC consumes about 2635 kJ of energy, which achieves a 15.7% improvement in energy efficiency and a 26.3% extension in battery life compared to the CS-3 with common IDM following strategy. These results indicate that the proposed T-ECC strategy has fulfilled the energy-saving pursuit while accounting for preceding vehicle interference in heavy traffic scenario.

To demonstrate the security guarantees of the SROC method, we also compare the following strategy with only the normal MPC. Fig. 15 depicts the following distance for the MPC-based car-following strategy. It can be observed that the general trend is similar to that of the SROC method. However, upon closer examination of the 12.6 km location in both Fig. 14 and Fig. 15, as highlighted in Fig. 16, a concern arises. In the MPC approach, the gap between vehicles narrows to below the safe minimum distance. In contrast, the SROC method avoids such a scenario, demonstrating the enhanced safety provided by our proposed SROC approach. In terms of computational burden, the single-step computation time of the benchmark is 20 ms, while the SROC method in T-ECC is 25 ms, which is comparable and showcase the potential of the proposed method for real-time implementation

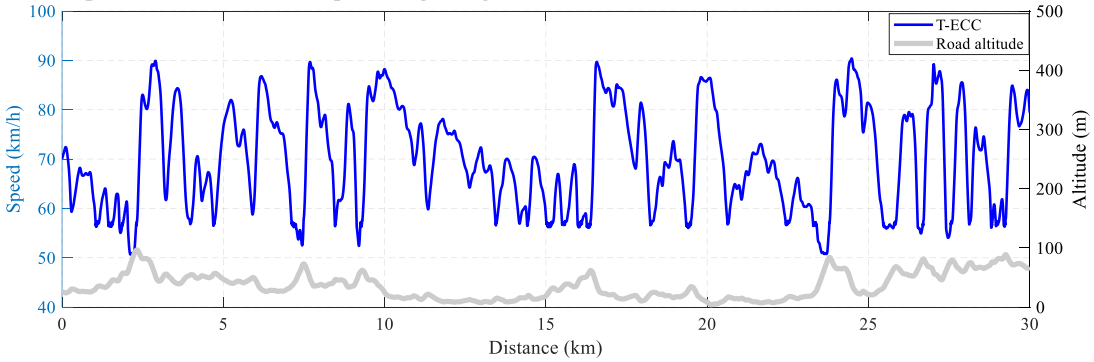

Fig. 9. Speed profiles of T-ECC.

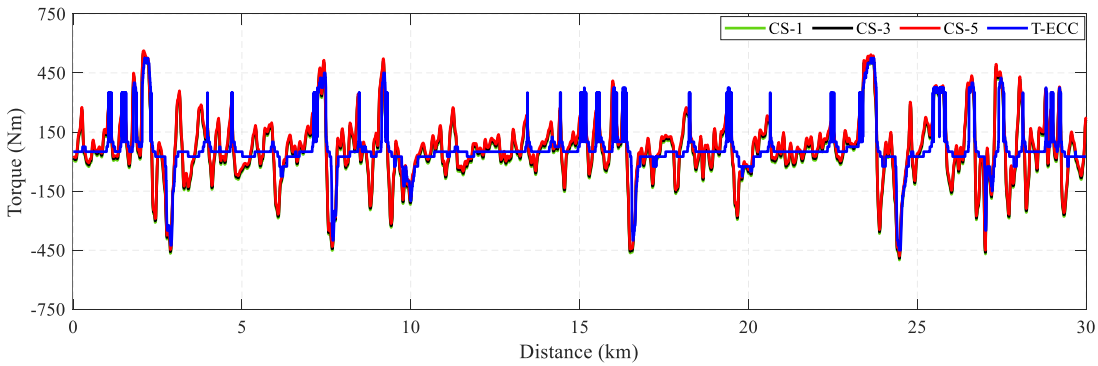

Fig. 10. Comparison of motor operating torques for the CS-1, CS-3, CS-5 and T-ECC.

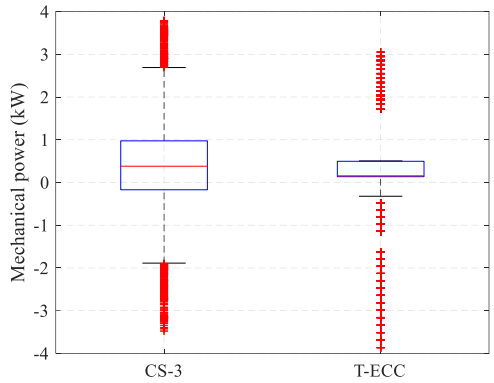

Fig. 11. Comparison of mechanical power of the motor for the CS-3 and T-ECC.

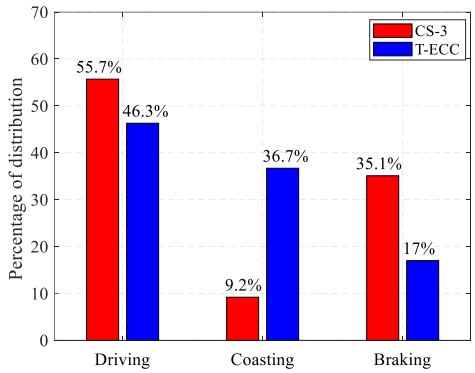

Fig. 12. Comparison of motor operating states distribution of the CS-3 and T-ECC.

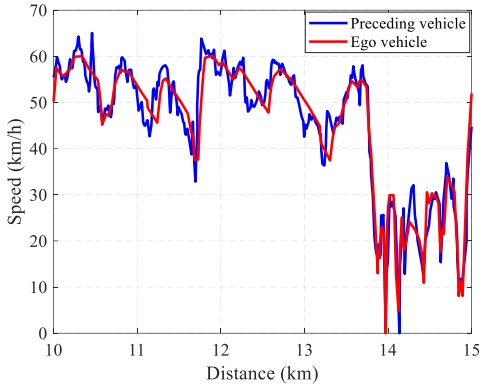

Fig. 13. Speed trajectory of the ego vehicle and preceding vehicle.

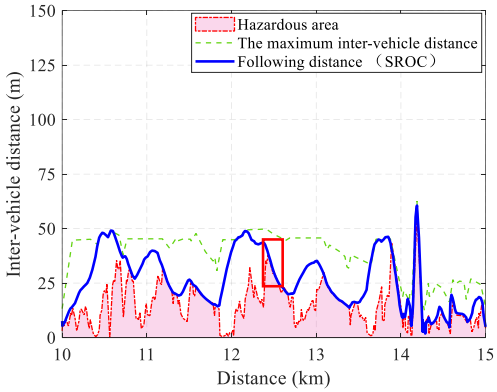

Fig. 14. Results for the following distance between the preceding vehicle and ego vehicle (SROC).

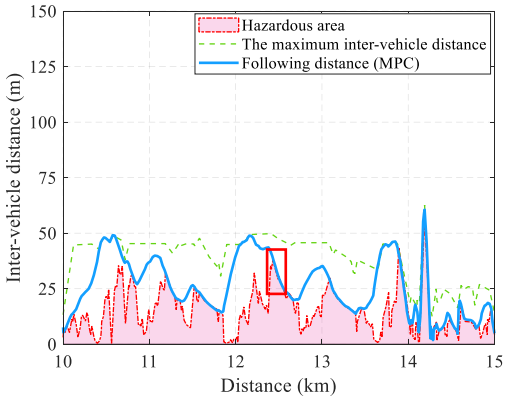

Fig. 15. Results for the following distance between the preceding vehicle and ego vehicle (MPC).

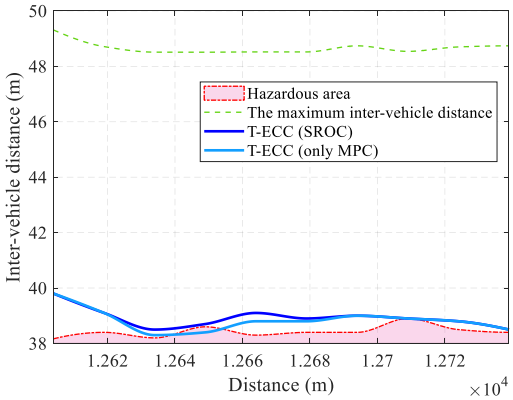

Fig. 16. Zoomed-in following distance by MPC and SROC in T-ECC.

TABLE III
COMPARISON OF THE RESULTS OF DIFFERENT STRATEGIES IN FREE-TRAFFIC SCENARIO

Strategies	Average speed	Energy consumption	Energy saving by T-ECC	Battery capacity loss	Battery life saving by T-ECC
CS-1	50 km/h	14142 kJ	-5.59%	0.0046%	8.70%
CS-2	60 km/h	15291 kJ	2.35%	0.0048%	12.5%
CS-3	70 km/h	16329 kJ	8.56%	0.0051%	17.6%
CS-4	80 km/h	17561 kJ	14.97%	0.0052%	19.2%
CS-5	90 km/h	18615 kJ	19.79%	0.0055%	23.6%
T-ECC	69.2 km/h	14932 kJ	--	0.0042%	--

3) *Stochastic traffic scenario*

To exhibit fully effectiveness of T-ECC, the results of 1000 sets of simulations are compared. The energy efficiency improvement and battery life extending of the T-ECC compared to the CS-3 in the 1000 stochastic simulation are shown in Fig. 17 and Fig. 18, respectively.

In Fig. 17, compared to CS-3, the energy efficiency improvements of T-ECC are concentrated between 7% and 16%, with a maximum energy savings of 20.98%. Fig. 18 reveals that maximum battery life extension of 35.17% can be realized by the T-ECC relative to the CS-3. In the 800 stochastic tests, the battery life improvement of T-ECC is predominantly

distributed around 20%. Further, the average energy efficiency improvement and battery life extension of the T-ECC are calculated in Table V, where we can see that the average energy economy of T-ECC under 1000 stochastic cases is enhanced by 11.37%, and meanwhile battery life is promoted by 20.03% in comparison to the CS-3. In summary, the above results highlight the energy economy and the ability to prevent battery degradation for the proposed strategy in random traffic scenarios, further confirming the adaptability and robustness of the T-ECC.

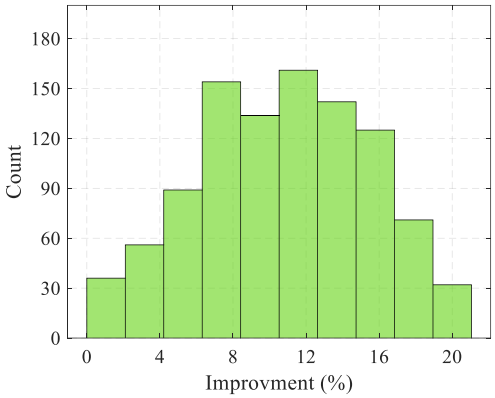

Fig. 17. Energy efficiency improvement during 1000 stochastic simulations.

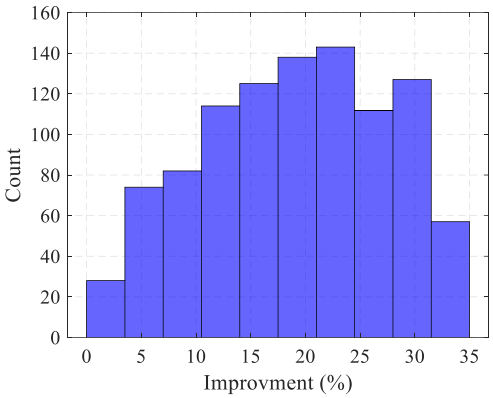

Fig. 18. Battery life improvement during 1000 stochastic simulations.

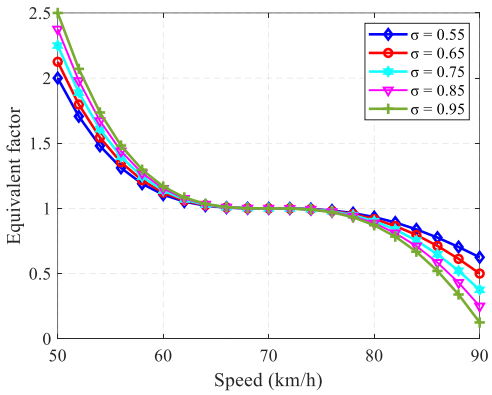

Fig. 19. EF curves with different σ values

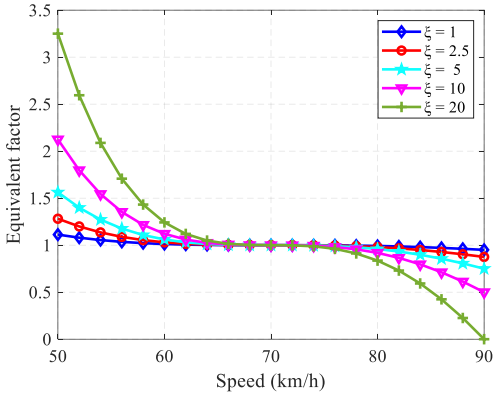

Fig. 21. EF curves with different ξ values.

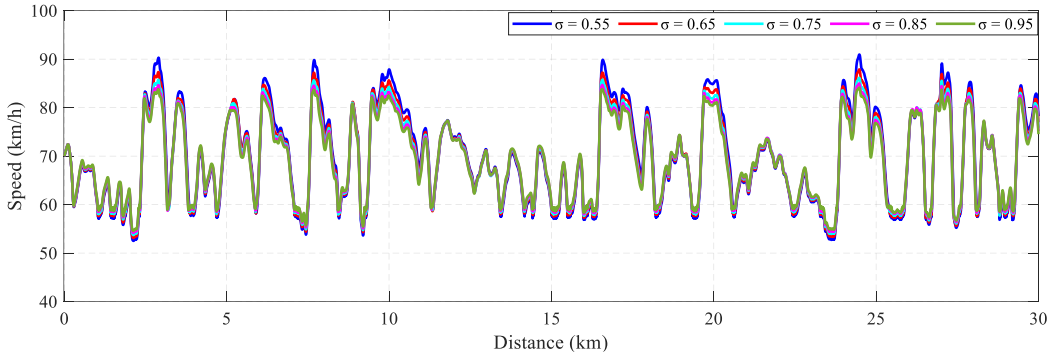

Fig. 20. Vehicle speed profiles with different σ.

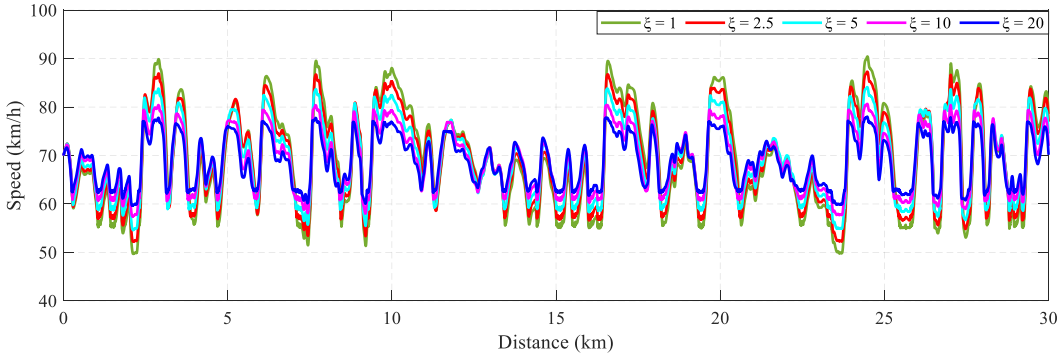

Fig. 22. Vehicle speed profiles with different ξ.

TABLE IV
RESULTS OF DIFFERENT FOLLOWING STRATEGIES IN HEAVY TRAFFIC SCENARIO

Strategies	Energy consumption	Energy saving	Battery capacity loss	Battery life saving
CS-3(IDM)	3216 kJ	15.7%	0.0019%	26.3%
T-ECC	2635 kJ		0.0014%	

TABLE V
AVERAGE ENERGY SAVINGS AND AVERAGE BATTERY LIFE EXTENDING DURING 1000 STOCHASTIC SIMULATIONS

Strategies	Average energy saving	Average battery life saving
CS-3 T-ECC	11.37%	20.03%

C. Sensitivity Analysis of Equivalent Factor

In this section, sensitivity analyses are performed to quantify the contribution of ξ and σ to the EF between kinetic energy and electricity consumption. We set the σ $(0.5 < \sigma < 1)$ as 0.55, 0.65, 0.75, 0.85, and 0.95, the EF curves and vehicle speed profiles with different σ are shown in Fig. 19 and Fig. 20 respectively. As depicted in Fig 19, the variation trend of the EF remains consistent across different values of σ, fluctuating around 1. It can be seen that the EF is relatively small at higher speeds, i.e., when the kinetic energy of the vehicle is higher, it is more desirable to replace the battery power consumption with body kinetic energy by reducing the kinetic energy conversion weights, and vice versa. Additionally, within the speed limit range of 50 to 90 km/h, the impact of σ on EF becomes more significant as it increases. Fig. 20 illustrates that the velocity profiles between 50 km/h and 90 km/h exhibit a high degree of similarity. Therefore, modifying the value of σ would have negligible effects on the cruising velocity profile within the low-speed range. However, noticeable discrepancies become apparent within the range of 80 to 90 km/h. When σ increases, the range of speeds becomes narrower, preventing the attainment of a top speed of 90 km/h due to an excessively large constant in the high-speed region.

Subsequently, we proceed with the other parameter analysis focusing on ξ, which is subject to the constraint $\xi \geqslant 1$. Five distinct values of ξ are chosen for evaluation: 1, 2.5, 5, 10, and 20. The variations of the EF corresponding to these different ξ values are graphically presented in Fig. 21. It can be seen that five lines exhibit notable variances, particularly within the range of 50 to 90 km/h. With an increase in ξ, the effect on the change rate of EF becomes more evident. It is noteworthy that the EF displays a higher sensitivity to the variable ξ compared to σ, meanwhile, the velocity profiles depicted in Fig. 22 demonstrate clear distinctions between them. In Fig. 22, as ξ increases within the range of 50 to 90 km/h, the minimum cruising speed rises, resulting in an upward shift of the lower limit of the speed range. Similarly, an increase in ξ leads to a decrease in the upper limit of cruising speed. When considering the overall cruise speed profile, larger values of ξ result in a narrower range of speeds for CEV.

V. VEHICLE-IN-THE-LOOP TEST

A. Vehicle Instrumentation

In this study, an eco-driving CEV platform is built composed of global navigation satellite system/inertial navigation system (GNSS/INS), millimeter-wave radar (MMW), LiDAR, and cameras, which is an organic combination of connected vehicle technology and autonomous driving shown in Fig. 23. Based on these in-vehicle sensing devices for acquiring road elevation, speed limit, and traffic information, the upper control system of the CEV experiment platform processes and fuses data from multiple sensors. It employs the proposed T-ECC algorithm to determine the underlying control commands of CEV and subsequently transmits them to the underlying actuators, enabling the execution of the vehicle's driving and braking operations in the autonomous driving mode, where the controller is executed at a frequency of 10 Hz. In the CEV platform, the software system based on the robotics operating system (ROS) is developed, connecting the drivers, data parsers and algorithms of the various components. Note that the ROS software platform is running on Ubuntu 16.04LTS and the framework is shown in Fig. 24.

Fig.23. The experimental platform and test road for the connected and automated vehicle.

In this real-world experiment, two vehicles with autonomous driving capabilities are used. The ego vehicle is based on the modified Chery Little-Ant, while the preceding vehicle we selected is a CEV that tracked a predetermined speed trajectory to depict controlled forward traffic behavior. The test is conducted on a closed road with a total length of 6000m. The first 4000 m simulates a free-flow traffic scenario without a preceding vehicle, representing an unrestricted traffic flow. At

the 4000 m of experimental road, a preceding vehicle appears, and the remaining 2000 m simulate a car-following scenario. This allows for the evaluation and testing of the ego vehicle's behavior in following the preceding vehicle.

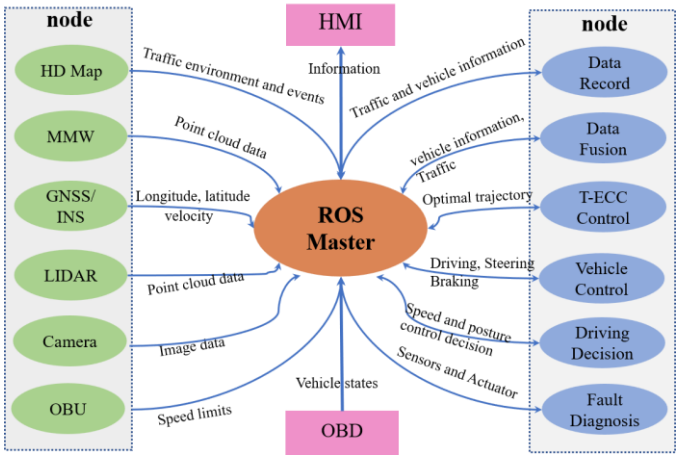

Fig. 24. A framework for ROS software.

TABLE VI

COMPARISON OF THE RESULTS OF T-ECC AND CS-3 IN THE EXPERIMENT

Strategies	Energy consumption	Energy saving
CS-3	2476 kJ	11.75%
T-ECC	2185 kJ	

Finally, the proposed T-ECC is validated and compared with the CS-3 strategy in the experiment, and the speed profiles and energy consumption comparisons for the two strategies are obtained in Fig. 25 and Table VI, respectively.

B. *Experimental Results*

In Fig. 25, it is demonstrated that T-ECC is capable of adjusting the vehicle speed based on changes in road gradient. Particularly in areas with significant slope variations, the speed variations are highly pronounced. It can be seen that the vehicle speed reaches its maximum at the lowest altitude point of the test road, i.e., at 1000 m, while at the highest altitude point, which is at 2500 m, the speed is at its minimum. These speed variations are accomplished through the implementation of SECS within T-ECC, enabling the vehicle to proactively accelerate before ascending a hill and effectively harnessing gravitational potential energy during descents. This approach mitigates the need for excessive braking, resulting in significant energy savings. In the heavy traffic scenario, both strategies effectively track the preceding vehicle. It can be observed that CS-3 utilizes the IDM to achieve vehicle following, resulting in a closer match to the motion state of the preceding vehicle. On the other hand, T-ECC maintains a dynamic gap for vehicle following. Therefore, when the ego vehicle decelerates, T-ECC proactively releases the accelerator pedal, allowing the vehicle to spend more time in a coasting state while ensuring safety and reducing energy consumption.

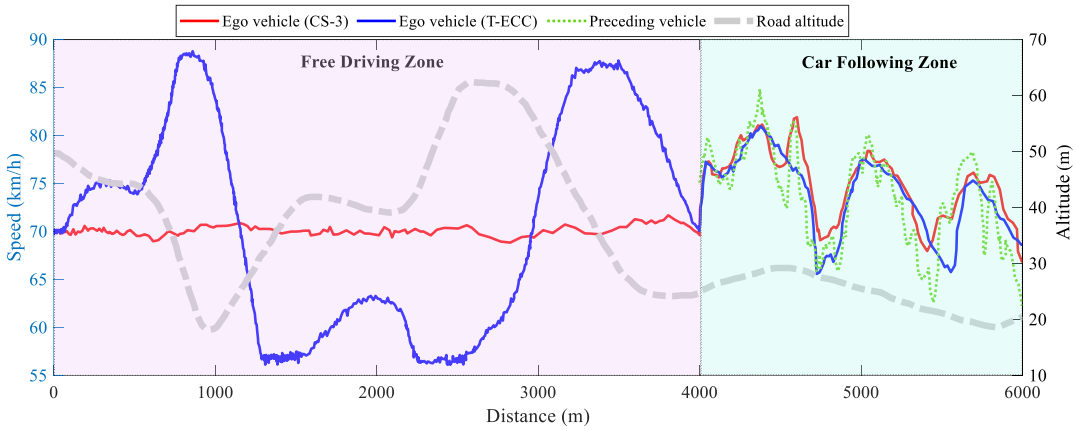

Fig.25. The velocity profiles by different methods in the experiment.

Throughout the entire experiment, the proposed T-ECC strategy only consumes 2185 kJ of energy, while CS-3 consumes 2476 kJ, resulting in an energy saving of 11.75%. Overall, the real-world experiment confirms the real-time performance and cost-effectiveness of the proposed T-ECC strategy.

VI. CONCLUSION

This paper proposes a T-ECC strategy based on the hierarchical framework for CEV operating in stochastic environments. By leveraging advantages of both long-term and short-term information integration, the strategy aims to improve energy efficiency. In the upper layer, a SECS strategy is proposed to generate a globally optimal energy-efficient speed. In the lower layer, the SROC method incorporating MPC and ACC is designed to track energy-optimal speed trajectory for CEV, simultaneously achieving synergistic optimization of energy efficiency, battery life, driving safety and driving comfort of ego vehicle in time-varying traffic conditions. Based on the stochastic traffic scenario constructed by the proposed stochastic preceding vehicle model, the simulation results confirm that T-ECC achieves an average of 11.37% energy saving and 20.03% battery life improvement compared to the improved CS strategy. Furthermore, a real vehicle implementation validated the real-time performance and economic benefits of the T-ECC strategy.

In the future, the T-ECC strategy will be tested under extreme road conditions and can be extended to a vehicular platoon consisting of a string of EVs in the context of V2V/V2I interactions.

REFERENCES

[1] G. Li, D. Görges, and M. Wang, "Online optimization of gear shift and velocity for eco-driving using adaptive dynamic programming," *IEEE Transactions on Intelligent Vehicles*, vol. 7, no. 1, pp. 123-132, 2021.

[2] J. Chen, Y. Ye, Q. Wu, R. Langari and C. Tang, "Low-Cost and High-Performance Adaptive Cruise Control Based on Inertial-Triggered Mechanism and Multi-Objective Optimization," *IEEE Trans Veh Technol.*, vol. 72, no. 6, pp. 7279-7289, June 2023.

[3] M. A. Silgu, *et al.*, "Network-wide emission effects of cooperative adaptive cruise control with signal control at intersections", *Transportation Research Procedia*, vol.47, pp. 545-552, 2020.

[4] S. Hulagu, H. B. Celikoglu, "An Electric Vehicle Routing Problem With Intermediate Nodes for Shuttle Fleets" *IEEE Trans Intell Transp Syst.* vol. 23, no. 2, pp. 1223-1235. Feb. 2022.

[5] L. Guo, *et al.*, "Cooptimization strategy of unmanned hybrid electric tracked vehicle combining eco-driving and simultaneous energy management,". *Energy.*, vol. 246, 2022, Art. no. 229916.

[6] D. Lang, R. Schmied, and L. Del Re, "Prediction of preceding driver behavior for fuel efficient cooperative adaptive cruise control," *SAE Int. J. Engines*., vol. 7, no. 2014-01-0298, pp. 14-20, Apr. 2014.

[7] M. Knowles, H. Scott, and D. Baglee, "The effect of driving style on electric vehicle performance, economy and perception," *Int. J. Electric Hybrid Veh.*, vol. 4, no. 3, pp. 228-247, Nov. 2012.

[8] M. Ozkan, Y. Ma, "Distributed stochastic model predictive control for human-leading heavy-duty truck platoon," *IEEE Trans Intell Transport Syst*., vol. 23, no. 9, pp. 16059-16071, Sep. 2022.

[9] C. Sohn, J. Andert, and D. Jolovic, "An analysis of the tradeoff between fuel consumption and ride comfort for the pulse and glide driving strategy," *IEEE Trans. Veh. Technol.*, vol. 69, no. 7, pp. 7223-7233, 2020.

[10] M. Wegener, *et al.*, "Automated eco-driving in urban scenarios using deep reinforcement learning," *Transp Res Part C: Emerg Technol.*, vol. 126, 2021, Art. no.102967.

[11] Y. Shao, Z. Sun, "Eco-approach with traffic prediction and experimental validation for connected and autonomous vehicles," *IEEE Trans. Intell. Transp. Syst*., vol. 22, no. 3, pp. 1562-1572, Mar. 2021.

[12] C. Sun, J. Guanetti, F. Borrelli, S. Moura, "Optimal eco-driving control of connected and autonomous vehicles through signalized intersections," *IEEE Internet Things J*., vol. 7, no. 5, pp. 3759-3773, May. 2020.

[13] S. Li, S. Xu, X. Huang, B. Cheng, H. Peng, "Eco-departure of connected vehicles with V2X communication at signalized intersections," *IEEE Trans Veh Technol*., vol. 64, no. 12, pp. 5439-5449, Dec. 2015.

[14] B. Asadi, A. Vahidi, "Predictive cruise control: utilizing upcoming traffic signal information for improving fuel economy and reducing trip time," *IEEE Trans Control Syst Technol*., vol. 19, no. 3, pp. 707-714, May 2011.

[15] S. E. Li, H. Peng, K. Li, and J. Wang. "Minimum fuel control strategy in automated car-following scenarios," *IEEE Trans. Veh. Technol.*, vol. 61, no. 3, pp. 998-1007, Jan. 2012.

[16] Q. Lin, S. Li, S. Xu, X. Du, D. Yang, K. Li, "Eco-driving operation of connected vehicle with V2I communication among multiple signalized intersections," *IEEE Intell Transp Syst Mag*., vol. 13, no. 1, pp. 107–119, Sep. 2021.

[17] X. Shan, C. Wan, and P. Hao, "Connected eco-driving for electric buses along signalized arterials with bus stops," *IET Intelligent Transport Systems.*, Vol. 17, no. 3, pp. 579-591, Mar. 2023.

[18] H. Dong, W. Zhuang, and B. Chen, "Predictive energy-efficient driving strategy design of connected electric vehicle among multiple signalized intersections," *Transp. Res. Part C: Emerg. Technol.,* vol. 137, pp. 106–120, Apr. 2022.

[19] Y. Yan, N. Li, and J. Hong., "Eco-Coasting Controller Using Road Grade Preview: Evaluation and Online Implementation Based on Mixed Integer Model Predictive Control," *IEEE Trans. Veh. Technol.,* DOI 10.1109/TVT.2023.3271656.

[20] S. Mousa, S. Ishak, R. Mousa, J. Codjoe, M. Elhenawy, "Deep reinforcement learning agent with varying actions strategy for solving the eco-approach and departure problem at signalized intersections," *Transp Res Rec*., vol. 2674, no. 8, pp. 119-131, Jul. 2020.

[21] J. Liu, W. Zhuang, H. Zhong, et al. "Integrated energy-oriented lateral stability control of a four-wheel-independent-drive electric vehicle," *Sci. China Technol. Sci.,* vol. 62, pp. 2170–2183, Dec. 2019.

[22] G. S. Ilgin, M. Menendez, and L. Meier. "Using connected vehicle technology to improve the efficiency of intersections," *Transport. Res. C*., vol. 46, no. 2, pp. 121-131, Nov. 2014.

[23] X. He, and X. Wu. "Eco-driving advisory strategies for a platoon of mixed gasoline and electric vehicles in a connected vehicle system," *Transport. Res. D-tr. E*., vol. 63, no. 5, pp. 907-922, Aug. 2018.

[24] L. Zhu, F. Tao, Z. Fu, N. Wang, B. Ji, and Y. Dong, "Optimization Based Adaptive Cruise Control and Energy Management Strategy for Connected and Automated FCHEV," *IEEE Trans Intell Transport Syst.*, vol. 23, no. 11, pp. 21620-21629, Nov. 2022.

[25] A. Bakibillah, *et al.*, "Event-driven stochastic eco-driving strategy at signalized intersections from self-driving data," *IEEE Trans Veh Technol*., vol. 68, no. 9, pp. 8557-8569, Sep. 2019.

[26] L. Li, X. Wang, and J. Song, "Fuel consumption optimization for smart hybrid electric vehicle during a car-following process," *Mech. Syst. Signal Process.*, vol. 87, pp. 17-29, Mar. 2017.

[27] N. Caroline, *et al.*, "Real-time eco-driving for connected electric vehicles," *IFAC-PapersOnLine*,Vol. 54, no. 10, pp. 126-131, 2021.

[28] D. Jia *et al.*, "An Enhanced Predictive Cruise Control System Design with Data-Driven Traffic Prediction," *IEEE Trans Intell Transport Syst*., vol. 23, no. 7, pp. 8170-8183, Jul. 2022.

[29] R. Lacombe, *et al.*, "Distributed Eco-Driving Control of a Platoon of Electric Vehicles Through Riccati Recursion," *IEEE Trans Intell Transport Syst*.,vol. 24, no. 3, pp. 3048-3063, Mar. 2023,

[30] L. Guo, B. Gao, Y. Gao, H. Chen, "Optimal energy management for HEVs in eco-driving applications using bi-level MPC," *IEEE Trans. Intell. Transp. Syst.*, vol. 18, no. 8, pp. 2153-2162, Aug. 2017.

[31] A. Bakibillah, M. Kamal, C. Tan, T. Hayakawa, and J. Imura, "Fuzzy-tuned model predictive control for dynamic eco-driving on hilly roads," *Appl Soft Comput*., vol. 99, 2021, Art. no. 106875.

[32] A. Bakibillah, M. Kamal, C. Tan, T. Hayakawa, J. Imura, "Eco-driving on hilly roads using model predictive control," in: *IEEE Joint 7th International Conference on Informatics, Electronics & Vision (ICIEV) and 2nd International Conference on Imaging, Vision & Pattern Recognition, icIVPR*, 2018, pp. 476–480.

[33] S. Xie, X. Hu, T. Liu, S. Qi, K. Lang, H. Li, "Predictive vehicle-following power management for plug-in hybrid electric vehicles," *Energy.*, Vol.166, no. 1, pp. 701-714, Jan. 2019.

[34] K. Luo, W. C. Zhuang, and L. Xu, "Energy-Efficient Feedback Control Strategy of Vehicle Platoon on Highway with Varying Slopes", *in Proc.CCC, Guangzhou, Guangdong, CA*, 2019.

[35] W. Zhuang, *et al.*, "Integrated energy-oriented cruising control of electric vehicle on highway with varying slopes considering battery aging," *Sci. China Technol. Sci.*, vol. 63, no. 1, pp. 155-165, Jan. 2020.

[36] S. Hulagu, H. B. Celikoglu, "Electric Vehicle Location Routing Problem WithVehicle Motion Dynamics-Based Energy Consumption and Recovery" *IEEE Trans Intell Transp Syst.* vol. 23, no. 8, pp. 10275-10286. Aug. 2022.

[37] V. Johnson, "Battery performance models in ADVISOR," *J.Power Sources.*, vol. 110, no. 2, pp. 321-329, Jun. 2002.

[38] J. Wang, *et al.*, "Cycle-life model for graphite-LiFePO4 cells," *J. Power Sources.*, vol. 196, no. 8, pp. 3942–3948, Apr. 2011.

[39] S. Bashash, "Extended horizon ECMS control of PHEVs with 2D electricity price adaptation policy," *IEEE Trans. Intell. Syst.*, vol. 18, no. 3, pp. 1-12, Jan. 2020.

[40] D. Fredette, U. Ozguner Dynamic, "Eco-Driving's Fuel Saving Potential in Traffic: Multi-Vehicle Simulation Study Comparing Three Representative Methods," *IEEE Trans Intell Transp Syst.* vol. 19, no. 9, pp. 2871-2879 9, Jan. 2018.

[41] H. Dong, W. Zhuang, B. Chen, "Enhanced Eco-Approach Control of Connected Electric Vehicles at Signalized Intersection with Queue Discharge Prediction," *IEEE Trans Veh Technol*., vol. 70, no. 6, jun. 2021.

[42] M. A. Silgu, I. G. Erdaˇgı, G. Göksu, and H. B. Celikoglu, "Combined Control of Freeway Traffic Involving Cooperative Adaptive Cruise Controlled and Human Driven Vehicles Using Feedback Control Through SUMO", *IEEE Trans Intell Transp Syst.* vol. 23, no. 8, pp. 11011-11025, Aug. 2022.

[43] M. A. Silgu, I. G. Erdaˇgı, *et al.*, "H_∞ State Feedback Controller for ODE Model of Traffic Flow", *IFAC-PapersOnLine*, vol. 54, no. 2, pp. 19-24. 2021.

[44] S. Goncu, I. G. Erdagi, M. A. Silgu and H. B. Celikoglu, "Analysis on Effects of Driving Behavior on Freeway Traffic Flow: A Comparative Evaluation of Two Driver Profiles Using Two Car-Following Models," *2022 IEEE Intelligent Vehicles Symposium (IV)*, Aachen, Germany, 2022, pp. 688-693, doi: 10.1109/IV51971.2022.9827296.

[45] C. Sun, J. Leng and F. Sun, "A Fast Optimal Speed Planning System in Arterial Roads for Intelligent and Connected Vehicles," *IEEE Internet Things J*., vol. 9, no. 20, pp. 20295-20307, Oct. 2022.

[46] Y. He, B. Ciuffo, Q. Zhou, "Adaptive Cruise Control Strategies

Implemented on Experimental Vehicles: A Review," *IFAC-PapersOnLine*, vol. 52, no. 5, pp. 21-27, 2019.
[47] Y. Zhang, Z. Chen, G. Li, "Integrated Velocity Prediction Method and Application in Vehicle-Environment Cooperative Control Based on Internet of Vehicles," *IEEE Trans Veh Technol*., vol. 71, no. 3, Mar. 2022.
[48] R. Firoozi, *et al*. "Safe Adaptive Cruise Control with Road Grade Preview and V2V Communication," *American Control Conference (ACC). IEEE*, pp. 4448-4453. 2019.
[49] S. Li, *et al*., "Strategies to minimize the fuel consumption of passenger cars during car-following scenarios,". *Proc Inst Mech Engineers Part D: J Automobile Eng.*, vol. 3226, no. 3, pp. 419-29. Oct. 2011.
[50] J. Han, A. Vahidi, A. Sciarretta, "Fundamentals of energy efficient driving for combustion engine and electric vehicles: An optimal control perspective," *Automatica*., vol. 103, pp. 558–572. May. 2019.

Bingbing Li received the M.S. degree in vehicle engineering from the School of Mechanical Engineering, Southeast University, Nanjing, China, in 2020. He is currently working toward the Ph.D. degree with Southeast University, Nanjing, China. His current research interests include connected and automated vehicles, energy-efficient driving, and vehicle dynamics control.

Weichao Zhuang (Member, IEEE) received the B.S. and Ph.D. degrees in mechanical engineering from the Nanjing University of Science and Technology, Nanjing, China, in 2012 and 2017, respectively. From 2014 to 2015, he was a Visiting Student with the Department of Mechanical Engineering, University of Michigan, Ann Arbor, MI, USA. He is currently an Associate Professor with the School of Mechanical Engineering, Southeast University, Nanjing.

His current research interests include, optimal control, clean energy vehicles, connected vehicles, and multiagent control.

Hao Zhang is currently a Ph.D. candidate at the School of Vehicle and Mobility, Tsinghua University, China. He works as a visiting researcher at the Department of Electronic and Electrical Engineering, University College London, U.K. His research interests include applications of optimal control to automotive engineering, in particular the reinforcement learning-based eco-driving and energy management of connected and automated hybrid electric vehicles.

Hao Sun received the B.Eng. in Mechanical Engineering from Shandong University, China in 2015 and the M.Sc. with distinction in Advanced Mechanical Engineering from the University of Warwick, UK in 2019. He has worked for two years at FAW-Volkswagen Automotive Co. Ltd and another two years at State Power Investment Corporation. He is currently working toward the Ph.D. in Electronic and Electric Engineering from University College London. His current research interests include distributed model predictive control, multi-agent system and autonomous driving.

Haoji Liu received the B.Eng. degree in vehicle engineering from Yanshan University, in 2019. He is currently pursuing the M.S. degree in vehicle engineering with the School of Mechanical Engineering, Southeast University. His research interests include vehicle motion planning, and cooperative control of connected and automated vehicles.

Jianrun Zhang received the Ph.D. degree in Mechanical Engineering from Southeast University, Nanjing, China, in 1997. From 1998 to 2000, He was a Postdoctoral Researcher with at the FIAT Research Center, Italy, and the Institute of Acoustics, Technische Universitat Berlin, Germany. He is currently a Professor with the School of Mechanical Engineering, Southeast University.

His current research interests include the vehicle dynamics and control, structural dynamic analysis, connected and automated vehicles, and optimization.

Guodong Yin (M'15-SM'20) received the Ph.D. degree in vehicle engineering from Southeast University, Nanjing, China, in 2007. From 2011 to 2012, he was a Visiting Research Scholar with the Department of Mechanical and Aerospace Engineering, Ohio State University, Columbus, OH, USA. He is currently a Professor with the School of Mechanical Engineering, Southeast University. He was the recipient of the National Science Fund for Distinguished Young Scholars.

His current research interests include vehicle dynamics and control, automated vehicles, and connected vehicles.

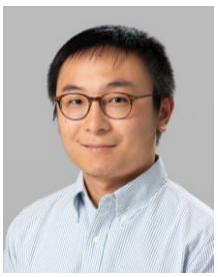

Boli Chen (Member, IEEE) received the B.Eng. degree in electrical and electronic engineering from Northumbria University, Newcastle upon Tyne, U.K., in 2010, and the M.Sc. and Ph.D. degrees in control systems from Imperial College London, London, U.K., in 2011 and 2015, respectively. He is currently a Lecturer with the Department of Electronic and Electrical Engineering, University College London, London, U.K.

His research interests include control, optimization, estimation and identification of a range of complex dynamical systems, mainly from automotive, and power electronics areas.